Numerical Analysis of Mixed-Phase Icing Cloud Simulations in the NASA Propulsion Systems Laboratory

Tadas P. Bartkus[1] and Jen-Ching Tsao[2]
Ohio Aerospace Institute, Cleveland, Ohio, 44135, USA

Peter M. Struk[3] and Judith F. Van Zante[4]
NASA Glenn Research Center, Cleveland, OH, 44135, USA

This paper describes the development of a numerical model that couples the thermal interaction between ice particles, water droplets, and the flowing gas of an icing wind tunnel for simulation of NASA Glenn Research Center's Propulsion Systems Laboratory (PSL). The ultimate goal of the model is to better understand the complex interactions between the test parameters and have greater confidence in the conditions at the test section of the PSL tunnel. The model attempts to explain the observed changes in test conditions by coupling the conservation of mass and energy equations for both the cloud particles and flowing gas mass. The model uses isentropic relations to relate gas temperature, velocity, density and pressure with respect to the PSL geometry. Measurements were taken at the PSL during wind tunnel tests simulating ice-crystal and mixed-phase icing that relate to ice accretions within turbofan engines in May 2015. The model was compared to experimentally measured values, where test conditions varied gas temperature, pressure, velocity and humidity levels, as well as the cloud total water content, particle initial temperature, and particle size distribution. Wet-bulb temperatures were generally within a few degrees of freezing. The model showed good agreement with experimentally measured values, to within approximately 30% of the measured change in gas temperature and humidity at the tunnel test section. The model did reasonably well in predicting melt content (liquid mass to total mass) at the test section, especially for clouds with larger particle sizes. In addition, the model predicted particle size at the tunnel exit with good agreement, however, the comparison was limited to clouds consisting of a small particle size distribution. One of the key findings from this work is that there was a nearly constant but slight increase in total wet-bulb temperature when the spray cloud was activated for every test and simulation. In addition, the total wet-bulb temperature in the tunnel plenum was a large factor in determining cloud phase.

Nomenclature

A	=	area (m^2)
a	=	speed of sound ($m\ s^{-1}$)
C	=	specific heat capacity ($J\ kg^{-1}\ K^{-1}$)
CDP	=	Cloud Droplet Probe (by Droplet Measurement Technology, Inc.)
C_D	=	coefficient of drag
d	=	particle diameter (m or μm)
Dv	=	volumetric diameter (m or μm)
$\dot{H}$	=	enthalpy rate (W)
h	=	heat transfer coefficient ($W\ m^{-2}\ K^{-1}$)
h_m	=	mass transfer coefficient ($m\ s^{-1}$)

[1] Senior Research Associate, Icing Branch, 21000 Brookpark Road, MS 110-3 AIAA Member.
[2] Principal Research Scientist, Icing Branch, 21000 Brookpark Road, MS 11-2, AIAA Associate Fellow.
[3] Aerospace Engineer, Icing Branch, 21000 Brookpark Road, MS 11-2, AIAA Member.
[4] Technical Lead - Icing, Facilities and Test Division, 21000 Brookpark Rd, MS 6-2, and AIAA Senior Member.

IRT = NASA Icing Research Tunnel
IWC = ice water content (g m^{-3})
k = ratio of specific heats of a gas
$\dot{KE}$ = kinetic energy rate (W)
L = latent heat of phase change (J kg^{-1})
LWC = liquid water content (g m^{-3})
MVD = median volume diameter (m or μm)
m = mass (kg)
NRC = National Research Council of Canada
P = pressure (Pa)
PSD = particle size distribution
PSL = NASA Propulsion Systems Laboratory
$\dot{Q}$ = heat flux (W)
RATFac = NRC's Research Altitude Test Facility
RH = relative humidity (%)
T = temperature or gas temperature (K, °C, or °F)
TP# = test point #
Twb = wet-bulb temperature (K, °C, or °F)
TWC = total water content (g m^{-3})
t = time (s)
v = velocity (m s^{-1})
x = distance (m)
Δ = change
∂ = differential
η = melt fraction (liquid water mass/total water mass)
ρ = density (kg m^{-3})
ω = mixed mass ratio (vapor mass/dry air mass)
= total number of particles in a bin

Subscripts
air = dry air
bulk = reference to bulk total water content
conv = convection
e = exit
exp = experiment
gas = gas
i = inlet condition or i^{th} number
in = in (into a control volume)
melt = melt
n = number of bins
noz = nozzle
on = spray on
off = spray off
out = out (out of a control volume)
p = particle (ice, water, or mixed phase)
ref = reference
s = static
sim = simulation
water = water
wv = water vapor
0 = total or plenum
%diff = percent difference

I. Introduction

SEVERAL jet engine power-loss events of commercial aircraft at high altitude have been reported since the 1990's. Mason et al.[1] discussed how power-loss could result from ice crystals entering the engine core, partially melting from the warm engine gas flow and refreezing on internal components. To better understand this phenomenon and determine the physical mechanism of icing in the core of the engine, NASA performed fundamental physics of ice-crystal ice accretion tests. A two-week test effort was conducted at the NASA Propulsion Systems Laboratory (PSL) in March 2016 with preliminary data collected in May 2015. During these tests it was critical to quantify key icing parameters at the test section, such as temperature, humidity, pressure, velocity, total water content, fraction of liquid to total water content, and the particle size distribution. The main objective of these tests was to generate a prescribed mixed-phase cloud at the test section.

During the PSL fundamental physics of ice-crystal icing tests, and on previous occasions[2-5], it has been observed that the test conditions, most notably temperature and humidity, change when the icing cloud is activated. In some cases, the gas temperature decrease was considerable, by as much as several degrees Celsius, accompanied by a measurable increase in water vapor. It is hypothesized that the ice particles and water droplets thermally interact with the flowing gas causing the gas temperature and humidity to change by the time the cloud particles reache the test section.

Existing thermal models[6-11] show little effect due to coupling of the ice/water particles with the flowing gas, or do not couple, approximating the gas mass as an infinite thermal reservoir with unchanging properties. A thermal model, previously written by Bartkus et al.[12] attempts to explain the observed changes in test conditions by coupling the conservation of mass and energy equations for both the ice/water particle and flowing gas mass. The model simulates both ice particle melting and droplet freezing, including spontaneous latent heat release during freezing for supercooled droplets. In the model, humidity changes are due to ice particle sublimation/deposition and water droplet evaporation/condensation. The associated latent heating/cooling and mass transfer change the ice water content (*IWC*) and liquid water content (*LWC*) from the moment of injection to the time the flowing mass reaches the test section. As a result, the model predicts changes in gas temperature, humidity, *IWC* and *LWC*, as well as the particle phase, size, temperature and velocity at the test section. To more accurately simulate spray injection, the model incorporates a distribution of particle sizes (24+ bins) as an initial input condition.

The model was specifically written to compare experimental data measured during a collaboratively conducted icing campaign between NASA GRC and the National Research Council of Canada (NRC) at the Research Altitude Test Facility (RATFac)[4, 5]. The model generally predicted the correct trend, but did not fully explain the changes that were observed at the RATFac icing wind tunnel. In general, the model was able to account for approximately 20% of the water that vaporized from the icing cloud, and approximately 20% of the gas temperature change that was observed experimentally[12]. One of the reasons offered for this discrepancy may be that water/ice film on the tunnel walls that had been observed during testing – which can increase vapor content and temperature change – was not accounted for in the model.

The NASA PSL is an altitude jet-engine test facility that generates ice particles using a liquid water spray nozzle system whereby the injected water droplets can freeze out as the cloud flows towards the engine/test section[13, 14]. The droplets freeze due to a combination of convective heat transfer and evaporative cooling. Unlike at RATFac, PSL can chose to not to deposit ice or water on the tunnel walls by turning off individual spray nozzles. This allows for a better platform for comparing the present thermal model – with modifications specific to the PSL – to experimentally measured data. The model has currently been modified to include isentropic relations with respect to the PSL geometry, which is described later in the paper. With this modification, the model aided in finding a range of conditions that resulted in a mixed-phase cloud at the exit of the PSL free jet duct during the 2015 and 2016 tests. Data measured during the recent March 2016 tests must still be analyzed, therefore this paper will only compare the data collected during preliminary testing in May 2015 with predicted model results. A detailed description of the preliminary 2015 testing, and an explanation of the data collected can be found elsewhere[15, 16].

II. Thermal Model Description

The thermal model simulates an icing wind tunnel by calculating particle and gas properties using expressions derived from the conservation of mass, momentum and energy equations. The particle mass and gas mass equations were fully coupled, as were the particle energy and gas energy equations. The conservation of momentum equation is solved only in reference to the particle, as it is approximated that the particles' effect on the flowing gas is negligible. Differential equations for change in gas temperature (T_{gas}), particle temperature (T_p), gas mass (m_{gas}), particle mass (m_p), gas velocity (v_{gas}), particle velocity (v_p), particle melt ratio (η_p), gas density (ρ_{gas}), and pressure (P) were derived

from equations of conservation. Since the tunnel geometry changes axially, isentropic relations were incorporated into the model to relate gas temperature, velocity, density and pressure with respect to changing are of the PSL geometry.

A. Assumptions

The thermal model operates under the following assumptions:

1) The values along the tunnel axis are steady (not a transient problem).
2) Gas and particle flow are steady and one dimensional.
3) The dry air and water vapor (that composes the gas) are treated as ideal gases.
4) Gas is well mixed, meaning that temperature, water vapor content and all thermodynamic properties are homogeneous within the gas control volume at any axial location (or time).
5) The system (tunnel) is adiabatic and mass is conserved.
6) Particle size distribution is characterized by a discrete set of diameters.
7) Particles of every size in the distribution are evenly spaced within the gas from the injection point to the test section (i.e. uniform total water content for a given cross-section).
8) All particles are perfectly spherical.
9) Particle aggregation/coalescences and breakup through collision are negligible.
10) Particles are injected in the direction of the flow and remain entrained with negligible gravity affects.
11) Temperature is uniform within the particle.
12) Mixed phase particles are spatially homogeneous in water/ice content. This means that evaporation and sublimation occurs from a mixed phase particle surface and the rate is determined by the water/ice content ratio. This applies to the reverse process of condensation and deposition as well.
13) Evaporation, sublimation, condensation and deposition occur at the particle surface at particle temperature.
14) The flow of particles and gas is a continuous stream. This means that while following a particular set of particles within a reference control volume, faster moving particles and gas that exit the reference control volume are replaced by thermodynamically identical particles and gas from a neighboring control volume that is upstream of the reference control volume. The reference control volume is centered on the slowest moving particle in a distribution of particles.

B. Thermal Model Equations – Gas Conservation Equations

The changing geometry of the tunnel must be addressed in the conservation of gas equations. The equations to follow refer to the infintesimal control volume in Figure 1. The volume is a representative of an infinetly thin cross-section of the tunnel. The flow is approximated to be one dimensional, flowing from left to right in Figure 1. With respect to nomenclature in this section, a parameter with a subscript of '*gas'*, refers to a property of the flowing gas (combined air and vapor), while the subscript, '*wv*', refers to a property of water vapor only. Also, the 'dot' accent, for example $\dot{m}$, refers to a rate.

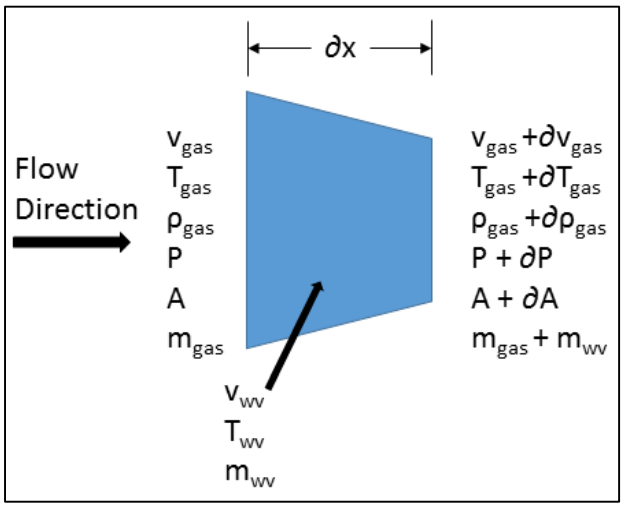

Figure 1: Differential control volume of width ∂x.

A unit mass of gas, m_{gas}, enters the control volume with a velocity of v_{gas}, a temperature of T_{gas}, a density of ρ_{gas}, and a pressure of P. Water vapor mass, m_{wv}, enters into the control volume as a mass source (or a sink if vapor is condensing), with velocity v_{wv} and temperature of T_{wv}. The gas and vapor masses enter the contol volume with an inlet surface area of A. At an infintesimal distance downstream, ∂x, the vapor mass exits the volume with velocity v_{gas} $\partial v_{gas,}$ a temperature of $T_{gas}+\partial T_{gas}$, a density of $\rho_{gas}+\partial \rho_{gas}$, and a pressure of $P+\partial P$. The gas exits the control volume with an exit surface area of $A+\partial A$.

Expressions that describe their changes through the infinitesimal volume for the five mentioned variables (v_{gas}, T_{gas}, ρ_{gas}, P, and A) are desired. Four of the five variables can be expressed using the conservation of mass, momentum and energy equations, along with the speed of sound equation. The fifth variable, the change in area, can be expressed using the known geomety.

The mass flow rate of the gas, $\dot{m}_{gas}$, can be expressed with respect to time, t, as shown in Eq. (1).

$$\dot{m}_{gas} = \frac{\partial m_{gas}}{\partial t} = \rho_{gas} A v_{gas} \tag{1}$$

Equation (2) shows the mass flow rate balance between the inlet and exit of the control volume. The water vapor mass flow rate, $\dot{m}_{wv}$, is treated as a mass source.

$$\rho_{gas} A v_{gas} + \dot{m}_{wv} = (\rho_{gas} + \partial\rho_{gas})(A + \partial A)(v_{gas} + \partial v_{gas}) \tag{2}$$

Equation (3) shows the gas momentum balance across the control volume. The expression below also approximates $v_{wv} = v_{gas}$, stating that the velocity of the vaporized gas is approximately the speed of the flowing gas.

$$\begin{aligned} &(\rho_{gas} A v_{gas}) v_{gas} + \dot{m}_{gas} v_{wv} + PA + (P + \partial P/2)\partial A \\ &= (\rho_{gas} + \partial\rho_{gas})(A + \partial A)(v_{gas} + \partial v_{gas})(v_{gas} + \partial v_{gas}) + (P + \partial P)(A + \partial A) \end{aligned} \tag{3}$$

The gas conservation of energy expression becomes a bit more complicated. Equation (4) shows the general gas energy rate balance between the inlet and exit of the infinitesimal volume. A subscript of '*in*' refers to an energy term entering the control volume, while a subscript of '*out*' refers to an energy term as it exits the control volume. The control volume is otherwise adiabatic. In the Eq. (4) below, $\dot{H}$ is the enthalpy rate term, $\dot{KE}$ is the kinetic energy rate term, and $\dot{Q}_{conv}$ is the convective heat transfer term between the particles and the flowing gas.

$$\dot{H}_{gas,in} + \dot{KE}_{gas,in} + \dot{H}_{wv,in} + \dot{KE}_{wv,in} + \dot{Q}_{conv} = \dot{H}_{gas,out} + \dot{KE}_{gas,out} + \dot{H}_{wv,out} + \dot{KE}_{wv,out} \tag{4}$$

The gas conservation of energy equation is expanded in Eq. (5) and also approximates $v_{wv} = v_{gas}$.

$$\begin{aligned} &\rho_{gas} A v_{gas} \left(C_{gas} T_{gas} + \frac{{v_{gas}}^2}{2}\right) + \dot{m}_{wv} \left(C_{wv} T_{wv} + \frac{{v_{gas}}^2}{2}\right) + \textcolor{blue}{\sum_{i=1}^{n} \pi d_i^2 h_i (T_{p,i} - T_{gas})(\#_i)} = \\ &\rho_{gas} A v_{gas} \left(C_{gas}(T_{gas} + \partial T_{gas}) + \frac{(v_{gas} + \partial v_{gas})^2}{2}\right) + \dot{m}_{wv} \left(C_{wv}(T_{gas} + \partial T_{gas}) + \frac{(v_{gas} + \partial v_{gas})^2}{2}\right) \end{aligned} \tag{5}$$

The convective heat transfer term, $\dot{Q}_{conv}$, in Eq. (4) is expressed in blue highlight in Eq. (5) as the sum of all the convective heat transferred from each individual particle size, *i*. In the above expression, n is the number of particle size bins and $\#_i$ is the number of particles in the i^{th} bin. T_p is the temperature of the particle, and h is the heat transfer coefficient for that particle. Also, C_{gas} and C_{wv} in Eq. (5) are the heat capacity of the gas and water vapor, respectively.

The speed of sound of a fluid, a, is expressed in Eq. (6), where k is the ratio of specific heats of a gas.

$$a^2 = \frac{\partial P}{\partial \rho_{gas}} = \frac{kP}{\rho_{gas}} \tag{6}$$

Equation (7) converts the conservation equations, which are normally temporally based, (i.e. $\partial/\partial t$), into spatially based expressions (i.e. $\partial/\partial x$). The variable geometry along the tunnel axis, which is known, can be expressed as a differential equation, where v_{ref} is the velocity of the reference frame. The reference frame for this model is the slowest moving particle velocity. The parameters in the tunnel are approximated to be steady state (i.e. not transient), and only vary in the axial direction.

$$\frac{\partial A}{\partial x} = \frac{\partial A}{\partial t}\frac{\partial t}{\partial x} = \frac{\partial A}{\partial t}\frac{1}{v_{ref}} \tag{7}$$

Combining and rearranging Eqs. (1), (2), (3), (6), and (7), while eliminating second order terms, provides expressions for the change in gas density, velocity and pressure across the infinitesimal volume and are given in Eqs. (8), (9) and (10) respectively.

$$\frac{\partial \rho_{gas}}{\partial x} = \frac{\rho_{gas} v_{gas} \left(\rho_{gas} A v_{gas} + \dot{m}_{wv}\right)}{\left(kPA - v_{gas}\left(\rho_{gas} A v_{gas} + \dot{m}_{wv}\right)\right)} \left(\frac{1}{A}\frac{\partial A}{\partial x} - \frac{1}{v_{ref}}\frac{\dot{m}_{wv}}{m_{gas}}\right) \tag{8}$$

$$\frac{\partial v_{gas}}{\partial x} = \frac{-kPAv_{gas}}{\left(kPA - v_{gas}\left(\rho_{gas} A v_{gas} + \dot{m}_{wv}\right)\right)} \left(\frac{1}{A}\frac{\partial A}{\partial x} - \frac{1}{v_{ref}}\frac{\dot{m}_{wv}}{m_{gas}}\right) \tag{9}$$

$$\frac{\partial P}{\partial x} = \frac{kPv_{gas}\left(\rho_{gas} A v_{gas} + \dot{m}_{wv}\right)}{\left(kPA - v_{gas}\left(\rho_{gas} A v_{gas} + \dot{m}_{wv}\right)\right)} \left(\frac{1}{A}\frac{\partial A}{\partial x} - \frac{1}{v_{ref}}\frac{\dot{m}_{wv}}{m_{gas}}\right) \tag{10}$$

Combining, and rearranging Eqs. (1), (5) and (7), while eliminating second order terms, provides an expression for the change in gas temperature across the infinitesimal volume and is given in Eq. (11).

$$\frac{\partial T_{gas}}{\partial x} = \frac{\rho_{gas} A v_{gas} \dot{Q}_{conv} - \dot{m}_{wv} \rho_{gas} A v_{gas} C_{wv} \left(T_{gas} - T_p\right) - v_{gas}\left(\rho_{gas} A v_{gas} C_{gas} + \dot{m}_{wv}\right) \frac{\partial v_{gas}}{\partial t}}{m_{gas} v_{ref} \left(\rho_{gas} A v_{gas} C_{gas} + \dot{m}_{wv} C_{wv}\right)} \tag{11}$$

Once again, the convective heat transfer term, $\dot{Q}_{conv}$, is the sum of all the individual heat transfers from all particles, as expressed and highlighted in blue in Eq. (5).

C. Thermal Model Equations – Particle Conservation Equations

The reader is encouraged to refer to the work by Bartkus et al.[12] for the derivation of equations that describe changes in the particle mass, velocity, temperature and liquid content. These equations, shown below, were derived from the particle conservation of mass, momentum and energy equations. The appendix of that reference also provides all of the air, water, ice, and vapor thermo-physical properties as functions of temperature, pressure, and humidity that are used in this model.

A mass balance is done for every particle size with the conservation of mass equation for particle size *i* shown in Eq. (12). In this equation, the subscript '*p*' refers to the particle. Also, *d* refers to the particle diameter, while h_m is the mass transfer coefficient.

$$\frac{\partial m_{p,i}}{\partial x} = \pi d_i^2 h_{m,i} \rho_{gas} \left(\omega_{gas} - \omega_{p,i}\right) \frac{1}{v_{ref}} \tag{12}$$

Equation (13) uses the conservation of momentum to provide an expression for the change in particle velocity across an infintesimal distance for every particle size *i*. In Eq. (13), C_D refers to the coefficient of drag.

$$\frac{\partial v_p}{\partial x} = \frac{3}{4} \frac{\rho_{gas} C_{D,i} \left(v_{gas} - v_{p,i}\right)^2}{\rho_{p,i} d_i} \frac{1}{v_{ref}} \tag{13}$$

The energy rate balance provides an expression for the change in particle temperature for every particle size *i* as shown in Eq. (14). In this equation, *h* refers to the heat transfer coefficient, while *L* is the latent heat of evaporation/condensation or sublimation/deposition.

$$\frac{\partial T_{p,i}}{\partial x} = \frac{6\left(\pi d_i^2 h_i \left(T_{gas} - T_{p,i}\right) + \pi d_i^2 h_{m,i} \rho_{gas} L_i \left(\omega_{gas} - \omega_{p,i}\right)\right)}{\pi d_i^3 \rho_{p,i} C_{p,i} v_{ref}} = \frac{6\left(\pi d_i^2 h_i \left(T_{gas} - T_{p,i}\right) + L_i v_{ref} \left(\frac{\partial m_{p,i}}{\partial x}\right)\right)}{\pi d_i^3 \rho_{p,i} C_{p,i} v_{ref}} \tag{14}$$

For a particle undergoing phase change, the conservation of energy provides an expression, Eq. (15), for the change in particle melt fraction, η, for every particle size i. In Eq. (15), L_{melt} refers to the latent heat of melting (i.e. latent heat of fusion).

$$\frac{\partial \eta_{p,i}}{\partial x} = \frac{6\left(\pi d_i^2 h_i\left(T_{gas}-T_{p,i}\right)+\pi d_i^2 h_{m,i}\rho_{gas}L_i(\omega_{gas}-\omega_{p,i})\right)}{\pi d_i^3 \rho_{p,i} L_{melt} v_{ref}} = \frac{6\left(\pi d_i^2 h_i\left(T_{gas}-T_{p,i}\right)+L_i v_{ref}\left(\frac{\partial m_{p,i}}{\partial x}\right)\right)}{\pi d_i^3 \rho_{p,i} L_{melt} v_{ref}} \quad (15)$$

Since mass is conserved, the change in particle mass is the opposite change in the gas mass. Mass loss due to evaporation from a particle, for example, is a gain in gas mass. Water vapor is treated like a source term in the gas conservation equations, Eqs. (2) - (5), and is the sum of all the mass transfers for each particle as expressed in Eq. (16).

$$\frac{\partial m_{wv}}{\partial x} = -\sum_{i=1}^{n}\left[\frac{\partial m_{p,i}}{\partial x}\right](\#_i) = \frac{\dot{m}_{wv}}{V_{ref}} \quad (16)$$

D. Instantaneous Condensation for Supersaturated Conditions

At the time of writing, the authors were uncertain about what happens when conditions in the tunnel can potentially exceed saturation near the tunnel exit. For example, elevated humidity levels in the tunnel inlet (plenum) can lead to supersaturation at the tunnel exit, due to a rapid static temperature decrease from isentropic expansion in the tunnel contraction. Condensation occurs if conditions are supersaturated, but only at the rate as physically allowed through diffusion. With higher speed flows, it was not clear if the vapor potentially in excess of saturation would condense (or deposit as ice) quickly enough to not exceed saturation.

For tests that may potentially exceed saturation, two simulations were run in an attempt to bound the problem, one where supersaturation was allowed, and one were the gas never exceeded saturation. For simulations that allow supersaturation, the equations as described in Sections II.B and II.C remain unchanged. For simulations that do not allow saturation to be exceeded, a subroutine was implemented that dealt with the mass that exceeded saturation which alters Eq. (12).

In order to not exceed saturation, the algorithm implemented instantaneous condensation (IC). For purposes of this paper, instantaneous condensation is referred to the amount of vapor mass that must condense in order to not exceed saturation; condensation rates faster than can occur through diffusion alone. In the model, no new particles were generated from IC; all condensation occurred on existing cloud particles only. For modeling simplicity, the IC mass was equally distributed among all of the existing cloud particles. The mass rate form of this distribution is shown in Eq. (17).

$$\dot{m}_{p,i} = \frac{\dot{m}_{wv}}{\sum_{i=0}^{n}(\#_i)} \quad (17)$$

In Eq. (17), $\dot{m}_{wv}$ is the vapor mass in excess of saturation, and is simply the $\dot{m}_{wv}$ value in Eqs. (8) - (11). Eq. (18) shows the above equation in terms of a differential with respect to x.

$$\frac{\partial m_{p,i}}{\partial x} = \frac{\dot{m}_{wv}}{V_{ref}\sum_{i=0}^{n}(\#_i)} \quad (18)$$

Equation (18) replaces Eq. (12) for calculating the changing particle mass. In addition, Equations (14) and (15) use this new mass increase as shown in the far right for each respective equation.

E. Thermal Model Algorithm

The thermal model was written in MATLAB version R2015b[17]. The model solves the differential equations of mass, momentum and energy transfer. All conservation equations presented in the following model formulation section are solved using MATLAB's built-in ODE45 solver. The system of differential equations is solved by first inputting the initial conditions. Time marching methods are employed by the MATLAB solver such that each iterative solution is solved with *numerical* relative and absolute tolerances of 10^{-8}. *Physical* accuracy of the solution is dependent on the accuracy of all the property values input into the model. For all simulations presented in this paper,

the energy transferred between the gas and particle(s) is balanced to the order of 10^{-4}. The mass transfer between the gas and particle(s) initial and final states is balanced to the order of 10^{-15}.

III. Model Sample - Input And Output

A. Experiment Descriptions

Figure 2 depicts the PSL geometry used for the 2015 tests. The PSL icing tunnel had a 27:1 area contraction ratio from the plenum (Tunnel Inlet) to the test section (Tunnel Exit), with an axial distance of about 8.84 m. The spray nozzles and spray bar system are located at the tunnel inlet in the plenum, while the test section is a 0.91 m (3.0 ft) diameter free jet exit. PSL has the capability to spray either de-ionized water or city water (i.e. water that was not treated). City was was used for all tests conducted, with an approximate freezing temperature of 0 °C (32 °F). The injected cloud covered most of the cross-sectional area at any point in the tunnel, but radial variations in total water content (*TWC*) and particle size distribution (PSD) likely exist. During a given test point, the facility generally maintained target pressures, temperatures and plenum relative humidites to approximately ±0.3 kPa (.05 psia), ± 0.5 °C (1 °F), and ± 1%, respectively[15].

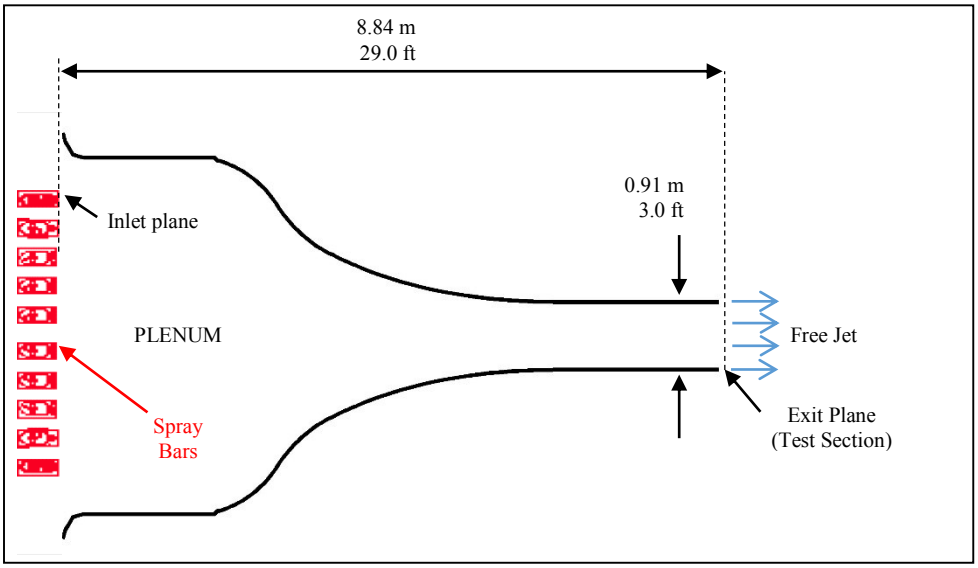

Figure 2: PSL tunnel geometry used for 2015 tests with spray nozzles located at the tunnel inlet while the temperature, humidity and water content measuring instruments were located near the tunnel exit.

Two experimental configurations are described for this paper and are shown in Figure 3. The first configuration was arranged to measure cloud content, gas temperature and humidity. Cloud content and phase were measured using the Science Engineering Associates (SEA) Multi-wire Probe[18-20] which was located on the tunnel centerline near the exit of the free jet. Gas temperature and humidity measurements were made with a probe that was placed near the exit of the free jet, with the probe inlet offset 0.25 m (9.7 in) from the centerline. Struk et al.[15] provides a description of the probe. In addition, all temperature, humidity and multi-wire data can be found in the same reference. Figure 3A shows the location of the multi-wire, and the combined temperature-humidity probe. A second configuration was arranged to measure particle sizes using a Cloud Droplet Probe (CDP) manufactured by Droplet Measurement Technologies, Inc. The probe was placed on the centerline axis near the exit of the tunnel and is pictured in Figure 3B. The CDP probe is capable of measuring particle sizes from 2 to 50 µm. Van Zante et al.[16] describes the configuration in greater detail and provides a summary of the cloud characterization. A description of the probe's operation is described by Van Zante and Rosine[14].

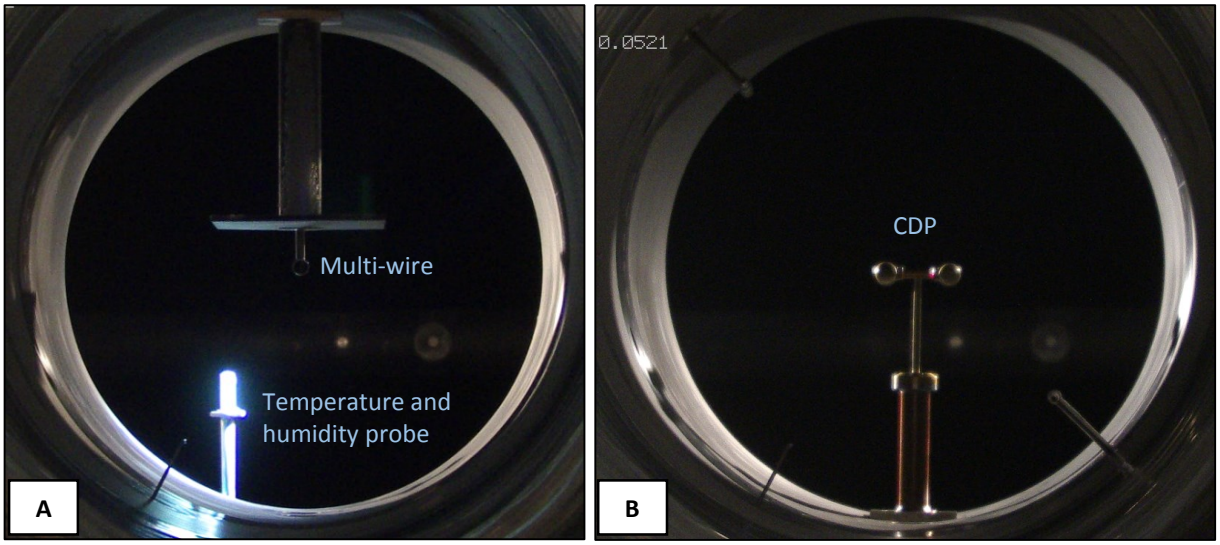

Figure 3: Image of two configurations used at PSL where A) the multi-wire and the combined temperature-humidity probe are shown in the first configuration and B) the particle size measuring CDP probe is shown in the second configuration. Images are taken from the plenum camera, forward-looking aft.

B. Model Input

Experimental conditions are needed as inputs for the model. The main gas parameters required are the inlet gas temperature, pressure, and relative humidity, as well as the gas velocity at the tunnel exit. The main cloud inputs needed are the inlet median volumentric diameter (*MVD*), total water content, and cloud temperature. In addition, an approximate initial cloud velocity is required since this does not model the immediate exit of the pressurized spray nozzles. All sprays are initially liquid. Finally, the tunnel geometry, previously described, is the final model input.

In order to more accurately simulate the cloud from the injection point just aft the spray nozzle bar system to the tunnel exit, an initial cloud PSD is required. The NASA PSL uses identical spray nozzles as in the NASA Icing Research Tunnel (IRT), and it is postulated that the measured PSD values at the NASA IRT test section are approximately equivalent to the initial PSD just aft of the nozzles at NASA PSL. PSD measurements were made in the IRT test section, but since the tunnel is a closed loop and near saturation, it is approximated that the PSD as it exits the IRT spray nozzles is the same PSD at the test section. PSDs of different cloud sizes were measured at the NASA IRT for various nozzle settings, namely the nozzle water pressure, $P_{water,noz}$, and nozzle atomizing air pressure $P_{air,noz}$[21]. For this work, three initial PSDs were used, with median volumetric diameters, *MVD*, of 15, 20 and, 40 μm respectively. Each distribution uses the PSD from the IRT and contains at least 24 bins.

C. Model Sample Results

Several parameter subscripts need to be defined, which will apply for the remainder of the document. Subscripts of '*0*' and '*s*' refer to a total or static value, respectively. A subscript of '*i*' refers to a parameter at the tunnel inlet, while a subscript of '*e*' refers to the tunnel exit. Conditions with a subscript of '*off*" refer to parameter values prior to the spray nozzles being activated, while a subscript of '*on*' refers to values when the spray is turned on. A subscript of '*exp*' refers to experimentally measured data, while '*sim*' refers to model simulation results.

Results from a simulation of Test Point # (TP#) 672 are provided as an example of the thermal interactions between the injected cloud and flowing gas. Figure 4 shows the predicted A) temperature, B) melt ratio, C) mass fraction that has evaporated, D) humidity along the tunnel axis, E) cloud residence time, and F) volumetric diameters. The inlet total temperature, $T_{0,i}$ = 277.3 K (39.5 °F), inlet total relative humidity, $RH_{0,i}$ = 10.8%, and inlet total pressure, $P_{0,i}$ = 87.5 kPa (12.7 psi), were used as initial inputs into the model. A gas velocity at the tunnel exit of v_e = 85 m/s was specified as a model parameter input. Liquid water was injected with an initial temperature of 280.4 K (45 °F) at a bulk total water content of TWC_{bulk} = 2.26 g/m^3. The value of TWC_{bulk} was calculated as the ratio of water mass flow rate to volumetric gas flow rate at the test section and is calculated using Eq. (19) below. In this equation $\dot{m}_{water}$ is the water mass flow rate, and A is the cloud effective area which is assumed to be the same as the tunnel exit (i.e. 0.91m diameter). This TWC_{bulk} value assumes that all injected water reaches the exit of PSL (i.e. no evaporation or condensation) and is uniformly distributed across the exit area. TWC_{bulk} is simply an input value whose value

changes as the cloud partially evaporates/sublimates before reaching the tunnel exit. The simulation used the $MVD_i = 40$ µm particle size distribution, a close representation of the approximate 42-µm cloud that was initially injected into the tunnel by the spray nozzles. The PSD used in this simulation contained 44 bins.

$$\mathrm{TWC}_{\mathrm{bulk}} = \frac{\dot{m}_{water}}{v_e A} \tag{19}$$

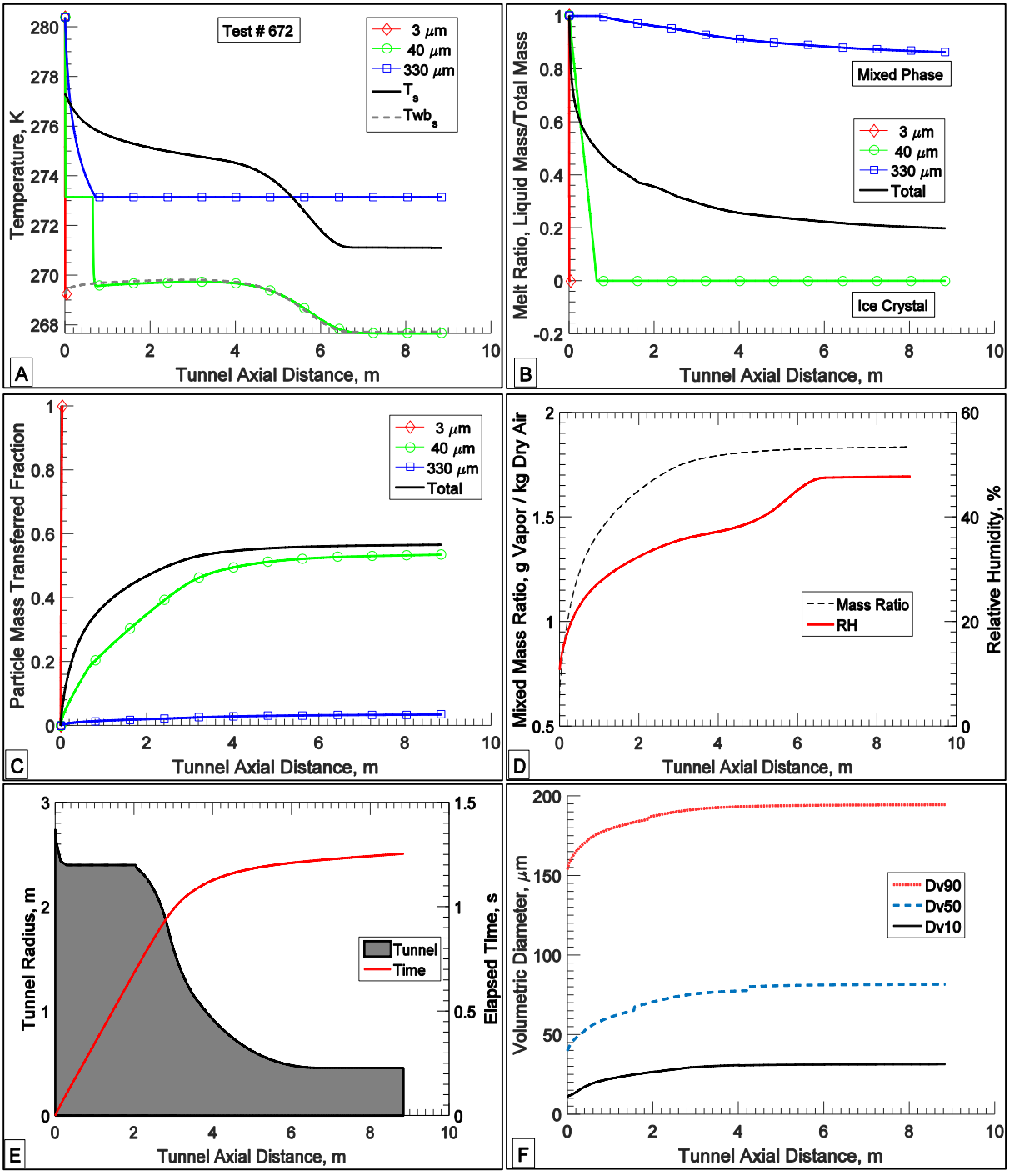

Figure 4: Simulation of TP# 672 where A) temperature, B) melt ratio, C) mass fraction that has evaporated, D) humidiy, E) residence time, and F) volumetric diamters are shown with respect to the tunnel axial distance.

Figure 4A shows the temperatures of three differently sized particles in the cloud, as well as the gas static temperature, $T_{s,sim}$, and static wet-bulb temperature, $Twb_{s,sim}$, along the axis of the PSL icing tunnel. The three particle sizes correspond to the smallest (dia = 3 μm), volumetric median (dia = 40 μm), and largest particle (dia = 330 μm) of the PSD used. The gas static temperature decreased from a combination of convective heat and mass transfer, as well as from isentropic expansion. With the cloud off, the gas static temperature at the tunnel exit calculates to be $T_{s,e,off,sim}$ = 273.7 K (33 °F), but with the cloud on, the gas temperature decreased to $T_{s,e,on,sim}$ = 271.1 K (28.3 °F). The simulation predicted a 2.6 K (4.7 °F) decrease in gas temperature at the tunnel exit with the cloud activated. Also, all particles in the cloud decreased in temperature from the initial injection particle temperature. The largest particle was mixed phase which reached a temperature of 273.15 K (32 °F) at the test section. After completely glaciating, the 40μm-particle (and all other particles that froze out but are not shown in the figure) reached the static wet-bulb temperaure, Twb_s. This can be seen in Figure 4A as the 40-μm particle follows the calculated wet-bulb temperature curve (gray dashed line). Wet-bulb temperature is the temperature of a wet adiabatic surface undergoing evaporation (or sublimation of ice). Twb_s is the resulting temperature when convective heat transfer is balanced by evaporative cooling and is a function of T_s, RH_s, and P_s [22]. The smallest particle (3 μm) quickly froze out and evaporated/sublimated completely away, within traveling a distance of 0.037m in the tunnel. This is expected as the large surface area to volume ratio for small particles encourages heat and mass transfer and will have a fast response.

Figure 4B shows the melt ratios, η, for the three differently sized particles as well as the summed total melt ratio for the entire cloud. Melt ratio is defined as the ratio of liquid content to total water content. For a liquid water droplet, the melt ratio equals 1, while a solid ice particle, the melt ratio equals 0. In the simulation, the largest particle began to freeze, but remained mixed phase, and largely liquid, by the tunnel exit. This slow transition in phase is expected because the small surface area to volume ratio for large particles dampens heat and mass transfer and will respond more slowly. The 40-μm particle glaciated completely by 0.65 m down the tunnel. The smallest particle began to freeze at a distance of 0.001m, became completely glaciated by 0.004 m and as mentioned before, vaporized completely by 0.037m. Summing the liquid and total masses of all remaining particles, the final melt fraction at the tunnel exit totaled $\eta_{e,sim}$ = 0.21.

Figure 4C shows the mass fraction that vaporized for each of the 3 different particle sizes and the summed total amount that vaporized from the cloud. A value of 1 indicates complete evaporation or sublimation, while a value of 0 means no mass change occurred. A negative value would indicate mass gain, through condensation or depostion. As expected, the largest particle experienced the least amount of mass loss due to its low surface area to volume ratio. Over half of the mass of the 40-μm particle vaporized, while as mentioned before, the smallest particle vaporized and reached the value of 1 quickly, at which point it disappeared. Approximately 56% of the total cloud mass vaporized completely by the tunnel exit.

Figure 4D shows the predicted mixed mass ratio, ω_{sim}, (black dashed line) and static relative humidity, $RH_{s,sim}$, (red solid line) for the flowing gas along the tunnel axis. Mixed mass ratio is defined as the ratio of vapor mass to dry air mass. Mixed mass ratio increased along the tunnel axis from 0.64 to 1.83 g/kg, due to particle evaporation and sublimation. $RH_{s,sim}$ increased as well, from a combination of added vapor content to the flowing gas and decrease in static gas temperature. With the cloud off, the static relative humidity at the tunnel exit calculated to be $RH_{s,e,off,sim}$ = 13.3%, but increased to $RH_{s,e,on,sim}$ = 47.6% with the cloud activated.

The shaded region in Figure 4E represents the tunnel geometry and is shown for positional reference. The red curve in Fig. 4E represents the amount of time that has elapsed for cloud particles that had been sprayed out of the nozzles to reach a particular axial distance in the tunnel. It took cloud particles 1.25 seconds to travel from the spray nozzles to the exit of the tunnel. It is important to note that the cloud resided in the plenum for approximately 1.0 seconds, or about 80% of the total time. The cloud particles resided in the plenum for so long because they were moving slowly at only a few meters per second in this section of the tunnel. The cloud particles accelerated through the contraction, and due to the elevated velocity, passed through the remaining tunnel section quickly. The largest changes in total gas temperature, melt fraction (freezing), mixed mass ratio (absolute humidity), and particle evaporation occurred in the plenum, since the cloud particles resided here for a substantial fraction of the time.

In an attempt to characterize the cloud particle size distribution, Figure 4F shows three volumetric diameters along the axis of the tunnel, *Dv10*, *Dv50*, and *D90*. Volumetric diameter is a representative diameter where the specified percentage of the total volume of the spray is composed of particles with diameters smaller than or equal to the stated value. For example, Dv10 is the diameter where 10% of the cumulative volume of the spray is made up of particles smaller or equal to the specified diameter. *Dv50*, which is by definition the *MVD*, signifies the diameter where half of the cumulative volume is composed of particles smaller than this diameter while the other half of the total volume is greater than this diameter. Finally, *Dv90* represents the diameter where 90% of the cumulative volume is smaller than the diameter calculated for *Dv90*. The *Dv10* and *Dv90* values provide a width of distribution, or a band around the

median *Dv50* value. All three *Dv* curves increased from their initial value, despite cloud mass loss due to evaporation/sublimation. In this example, *Dv50* increased from 40μm to 82μm from the tunnel inlet to the exit. This increase in *Dv* is caused by smaller particles completely evaporating, leaving only the larger particles. Smaller particles have a greater surface area to volume ratio and evaporated more quickly than larger particles. Even though these remaining large particles were smaller than their initial size, the mathematical calculation of the three *Dv* values increased for this time period. It should be noted that provided enough time and the proper conditions to evaporate even the largest particles, the *Dv* curves would eventually all decrease to 0 μm.

IV. Model – Experiment Comparisons and Discussions

The focus of the May 2015 testing was to examine the effect various PSL facility parameters have on the melt ratio of the cloud at the test section. Three primary parameters were examined: bulk TWC, plenum humidity, and spray bar water temperature. Within these sets of results, target particle size was also varied between a smaller, nominally 15-μm MVD_i, and larger value of 40-μm MVD_i. Model results for each of these test variations are discussed in separate sections below. Model results are also compared with experimentally measured particle size data in a separate section.

A. Total Water Content Sweeps and Comparisons

For the rest of the document, any references to temperature in refer to the gas temperature, and the subscript of '*gas*' is omitted for ease of reading. Table 1 below shows the results of two sets of tests where bulk total water content, TWC_{bulk}, was varied. Facility target conditions are presented at the top half of the table for each test set, which includes the inlet total pressure, $P_{0,i}$, static pressure at the tunnel exit, $P_{s,e,off}$, gas velocity at the test section, V_e, inlet total temperature, $T_{0,i}$, and static temperature at the tunnel exit, $T_{s,e,off}$. The value of $P_{0,i}$, is approximated to be constant for the entire length of the tunnel and is independent of spray on or spray off conditions. Also, $P_{s,e,off}$ is approximated to be independent of spray on or spray off condition at the tunnel exit, and can also be written as $P_{s,e}$. The relative humidity in the icing tunnel plenum was specified during testing, which is a close approximation for the total relative humidity, $RH_{0,i}$, in the slow moving plenum. The corresponding mixed mass ratio in the plenum, ω_i, is also provided. From the temperature, humidity and pressure values, the total wet-bulb temperature, $Twb_{0,i,off}$, and the static wet-bulb temperature, $Twb_{s,e,off}$ are provided. Wet-bulb temperatures were calculated using equations as defined in Veres et al.[22]. The above parameters are facility target conditions in the absence of the icing cloud. The initial cloud characteristics (immediately aft the spray nozzles) are given in the table, which include the bulk total water content, TWC_{bulk}, initial water temperature, $T_{water,i}$, and initial cloud median volumetric diameter, MVD_i. The MVD_i was calculated using specified nozzle conditions, namely the nozzle water pressure, $P_{water,noz}$, and nozzle atomizing air pressure $P_{air,noz}$[21].

The bottom half of the table compares model results with experimentally measured values. The focus is on the change in experimental conditions when a cloud is present. The change in mixed mass ratio between cloud on and off was experimentally measured, $\Delta\omega_{exp}$. The corresponding simulation value, $\Delta\omega_{sim}$, is given, as well as how closely the simulated value matches the experimentally measured value, $\Delta\omega_{\%diff}$. The value of $\Delta\omega_{\%diff}$ is calculated as the following:

$$\Delta\omega_{\%diff} = \frac{\Delta\omega_{sim} - \Delta\omega_{exp}}{\Delta\omega_{exp}} \times 100\% \tag{20}$$

The change in gas total temperature at the test section between cloud on and off, $\Delta T_{0,e,exp}$, is provided, along with the corresponding simulated value, $\Delta T_{0,e,,sim}$. Similarly, the measure of how closely the simulated value matches the experimental value is given as $\Delta T_{0,e,\%diff}$, and is calculated as follows:

$$\Delta T_{0,e,\%diff} = \frac{\Delta T_{0,e,sim} - \Delta T_{0,e,exp}}{\Delta T_{0,e,exp}} \times 100\% \tag{21}$$

In Eqs. (20) and (21) a negative value means the simulation under-predicted the experimentally measured change, while a positive value means the model over-predicted the change.

The melt ratio is defined as the mass ratio of liquid water content to total water content. The experimentally measured melt ratio, $\eta_{e,exp}$, and simulation value, $\eta_{e,sim}$, at the tunnel exit are provided. The $\eta_{e,exp}$ value was calculated by taking the maximum value between the two LWC wires of the multi-wire (the 2.1 mm and 0.5 mm wires) and

dividing by the measured value from the TWC wire (the half-pipe)[15]. No correction factors were applied, as only the ratio of the raw measurements from the multi-wire are reported. Finally, the change in total wet-bulb temperature at the test section between cloud on and off, $\Delta Twb_{0,e,exp}$, is given, as well as the corresponding simulation value, $\Delta Twb_{0,e,sim}$.

Table 1: Total Water Content Data Set 1 Sweeps

Test Series →	***TWC Sweep 1***				***TWC Sweep 2***		
Facility Target Conditions							
$P_{0,i}$ (kPa)	87.2				44.6		
$P_{s,e,off}$ (kPa)	83.7				42.8		
v_e (m/s)	85				85		
Altitude (km)	1.6				6.8		
$T_{0,i}$ (°C)	6.6				6.1		
$T_{s,e,off}$ (°C)	3.0				2.5		
$RH_{0,i}$ (%)	10				10		
ω_i (g/kg)	0.70				1.3		
$Twb_{0,i,off}$ (°C)	-2.0				-5.6		
$Twb_{s,e,off}$ (°C)	-4.2				-7.4		
TWC_{bulk} (g/m^3)	0.55	1.0	2.2	3.5	0.55	1.0	2.3
$P_{air,noz}$ (kPa, gauge)	103	207	414	414	103	207	207
MVD_i (µm)	15				15		
$T_{water,i}$ (°C)	7				7		
Simulation vs Experimental Measurement Comparison							
TP#	666	667	665	664	678	679	680
$\Delta\omega_{e,exp}$ (g/kg)	0.71	1.3	2.1	2.1	1.4	1.7	2.8
$\Delta\omega_{e,sim}$ (g/kg)	0.51	0.9	2.0	2.7	1.0	1.8	3.7
$\Delta\omega_{e,\%diff}$ (%)	-28%	-26%	-7%	31%	-26%	6%	32%
$\Delta T_{0,e,exp}$ (°C)	-1.8	-3.0	-5.1	-4.8	-3.2	-4.4	-6.9
$\Delta T_{0,e,sim}$ (°C)	-1.2	-2.3	-4.7	-6.5	-2.5	-4.5	-8.9
$\Delta T_{0,e,\%diff}$ (%)	-33%	-24%	-8%	36%	-22%	3%	29%
$\eta_{e,exp}$ (-)	0.79	0.16	0.10	0.10	0.27	0.19	0.08
$\eta_{e,sim}$ (-)	0.00	0.00	0.00	0.00	0.00	0.00	0.00
$\Delta Twb_{0,e,exp}$ (°C)	0.1	0.3	0.4	0.6	0.3	0.2	0.5
$\Delta Twb_{0,e,sim}$ (°C)	0.1	0.2	0.4	0.7	0.2	0.3	0.7

Between the two data sets, experiments were conducted at a higher ambient pressure in the first data set, *TWC Sweep 1*, which also meant higher wet-bulb temperatures. The initial cloud size for each test was MVD_i = 15µm. In both sweeps, the experimentally measured vapor content increased at the test section as TWC_{bulk} increased. Simulations matched this humidity trend within approximately 30% of experimentally measured change for all 7 tests. As TWC_{bulk} increased, the drop in gas temperature generally increased. The model similarly matched this temperature trend to within approximately 30% of the measured change for all 7 tests. Comparing similar conditions from the two data sets, namely TP# 666, 667, and 665 vs TP# 678, 679, and 680 respectively, it can be seen that the increase in humidity was greater for the lower ambient pressure tests. Similarly, the decrease in temperature was greater for the lower pressure data set. These trends were expected and predicted by simulation as there is greater potential for evaporation at lower pressures.

For *TWC Sweep 1*, all simulations predicted a fully glaciated cloud. For the two higher TWC_{bulk} tests of *TWC Sweep 1* (TP# 665 and 664), the $\eta_{e,exp}$ was measured as 0.10. Such a low value suggests a mostly or fully glaciated cloud since a fully glaciated cloud produces a signal (~5% of IWC) on the LWC elements of the multi-wire resulting in a non-zero η. For the two lower TWC_{bulk} tests, in particular TP# 666, higher $\eta_{e,exp}$ values were measured, suggesting a mixed phase cloud. All things being equal, it is not expected to see a more liquid cloud as the TWC_{bulk} decreases, and in fact, the $\eta_{e,exp}$ measurement is expected to be more glaciated as TWC_{bulk} decreases. It is hypothesized that the resulting particle size distribution, for TP# 666 in particular, may have had a heavier right tail particle size distribution than what was used for simulation. While according the IRT particle size distribution calculator[21] the nozzle settings produce a 15-μm cloud, the atomizing air pressure of $P_{air,noz}$ = 103 kPa (15 psig) was lower for TP# 666 than the rest in the data set. As a result, the choked flow in the nozzle produced a weaker resulting shock , or expansion fan waves[23], as the gas expanded out of the nozzle compared to the greater pressurized nozzle tests.This weaker shock may have resulted in a greater number of larger particles, which would not have frozen out as quickly as smaller particles. In addition, there is a tendency for larger particles to concentrate towards the center of the tunnel, due to a combination of particle inertia and tunnel contraction. The multi-wire was measuring the melt ratio values at precisely the tunnel center and may also have contributed to this higher $\eta_{e,exp}$ measurement for TP# 666. Particle size measurements were not made for these tests or any of the parameter sweeps, so as to help verify this hypothesis.

Similarly, all three simulations predicted full glaciation for *TWC Sweep 2*. While TP# 680 suggests a mostly or fully glaciated cloud, the two lowest TWC_{bulk} tests, TP# 678 and 679, measured mixed phase clouds. Again, the atomizing air pressure, in particular TP# 678 was low, $P_{air,noz}$ = 103 kPa (15 psig), which when expanded out of the nozzle created a weaker shock that generated some large particles that may not have fully glaciated. This may account for the mixed phase experimental value, even though it is not expected for this low TWC_{bulk} case. One thing to note is that the experimentally measured melt ratio of TP# 678 ($\eta_{e,exp}$ = 0.27) is lower than its similar counterpart TP# 666 ($\eta_{e,exp}$ = 0.79). Since TP# 678 was conducted in a lower ambient pressure, more evaporative cooling occurred, which reduced the melt ratio slightly more than the higher pressure companion test.

A trend is recognizable in wet-bulb temperature, *Twb,* as well. As TWC_{bulk} increased, an increase in $\Delta Twb_{0,e,exp}$ was measured, which was also predicted by simulation. The increase was not large as there was a near balance in the calculated *Twb* using the pre-spray humidity and temperature and the calculated *Twb* value during spray-on where there was an increase in vapor and decrease in gas temperature from evaporating particles. This increase in ΔTwb_0 is attributed to the energy added to the system from an initial water temperature that was greater than the wet-bulb temperature. An assertion made for calculating wet-bulb temperature is that the evaporating water temperature is supplied at the wet-bulb temperature. For an unsaturated, adiabatic system where the water temperature is greater than *Twb*, the calculated wet-bulb temperature will increase and the final *Twb* value will be dependent on the amount of water mass (or more specifically, the amount of energy associated with the water mass) in the system. Hence, higher TWC_{bulk} experiments in Table 1 provided more energy to the gas since $T_{water} > T_{wb}$ for every test, which resulted in greater $\Delta Twb_{0,e}$ values compared to lower TWC_{bulk} tests for a given *TWC* sweep.

In addition to the change in wet-bulb temperature, information on the state of the cloud can be gleaned from the absolute *Twb*. For example, the total and static wet-bulb temperatures for *TWC Sweep 1*, $Twb_{0,i,off}$ = -2.0 °C (28 °F) and $Twb_{s,e,off}$ = -4.2 °C (24 °F) respectively, were both below freezing. This means that once injected into the tunnel plenum, the evaporating particles experienced sub-freezing conditions, even with an approximate 0.5 °C (~1 °F) increase in total wet-bulb temperature. With a freezing point of 0 °C (32 °F) for city water, it is expected to see a fair amount of glaciation, especially for clouds composed of smaller particles such as in these two data sets.

Table 2: Total Water Content Data Set 2 Sweeps

Test Series →	***TWC Sweep 3***				***TWC Sweep 4***			
Facility Target Conditions								
$P_{0,i}$ (kPa)	87.3				87.3			
$P_{s,e,off}$ (kPa)	83.6				83.6			
v_e (m/s)	85				85			
Altitude (km)	1.6				1.6			
$T_{0,i}$ (°C)	4.2				1.8			
$T_{s,e,off}$ (°C)	0.6				-1.8			
$RH_{0,i}$ (%)	10				10			
ω_i (g/kg)	0.60				0.50			
$Twb_{0,i,off}$ (°C)	-3.3				-5.0			
$Twb_{s,e,off}$ (°C)	-5.6				-7.2			
TWC_{bulk} (g/m^3)	0.78	1.4	2.3	5.0	0.78	1.4	2.3	5.1
$P_{air,noz}$ (kPa, gauge)	55	103	207	207	55	103	207	207
MVD_i (µm)	40				40			
$T_{water,i}$ (°C)	7				7			
Simulation vs Experimental Measurement Comparison								
TP#	670	671	672	673	677	676	675	674
$\Delta\omega_{e,exp}$ (g/kg)	0.55	0.87	1.3	2.3	0.49	0.85	1.3	2.1
$\Delta\omega_{e,sim}$ (g/kg)	0.45	0.75	1.2	2.3	0.43	0.72	1.1	2.1
$\Delta\omega_{e,\%diff}$ (%)	-19%	-13%	-11%	0%	-12%	-16%	-14%	3%
$\Delta T_{0,e,exp}$ (°C)	-1.7	-2.3	-2.9	-3.7	-1.7	-2.1	-1.8	-3.8
$\Delta T_{0,e,sim}$ (°C)	-1.0	-1.7	-2.7	-4.8	-0.9	-1.6	-2.5	-4.3
$\Delta T_{0,e,\%diff}$ (%)	-41%	-27%	-7%	28%	-45%	-27%	39%	13%
$\eta_{e,exp}$ (-)	0.69	0.66	0.23	0.27	0.70	0.67	0.19	0.20
$\eta_{e,sim}$ (-)	0.20	0.19	0.20	0.20	0.12	0.11	0.11	0.11
$\Delta Twb_{0,e,exp}$ (°C)	-0.1	0.1	0.5	1.4	-0.2	0.1	1.1	1.1
$\Delta Twb_{0,e,sim}$ (°C)	0.1	0.3	0.4	0.9	0.2	0.3	0.4	1.0

Two series of TWC_{bulk} sweeps are presented in Table 2, where the target total temperature of *TWC Sweep 3* is about 2.4°C (4°F) warmer than *TWC Sweep 4*. The initial cloud MVD_i for each test was 40 µm. As was the case before, the experimentally measured vapor content increased as TWC_{bulk} increased. Simulations matched this humidity trend within approximately 20% of experimentally measured change for all 8 tests. Again, as TWC_{bulk} increased, the drop in gas temperature generally increased. The model similarly matched this temperature trend to within approximately 40% of the measured change for all 8 tests. Comparing similar conditions from the two data sets in Table 2, it can be seen that the increase in humidity was slightly greater for the warmer test set. Similarly, the decrease in temperature was slightly greater for the warmer data set. These trends were expected and predicted by simulation as there is greater potential for evaporation at warmer temperatures. The differences were small perhaps due to the fact that the 2.4 °C (4 °F) between the two data sets in Table 2 is not a large difference.

Simulations predicted a melt ratio of approximately $\eta_{e,sim} = 0.20$ for all 4 tests runs in *TWC Sweep 3*, regardless of TWC_{bulk}. This value matches very closely the melt ratio measured for the for the two higher *TWC* tests, TP# 672 and TP# 673, where $\eta_{e,exp} = 0.23$ and $\eta_{e,exp} = 0.27$ respectively. As was the case before, a lower TWC_{bulk} should not result in a more liquid cloud, but this was the case for TP# 670 and TP# 671 where $\eta_{e,exp} = 0.69$ and $\eta_{e,exp} = 0.66$ respectively. Again, it is speculated that the lower nozzle air pressure settings for the lower TWC_{bulk} tests produced a heavier right tail PSD than what was used for simulation. The same trend appears again for *TWC Sweep 4*. The model predicts quite

well the melt ratio for the higher TWC_{bulk} tests, but not for the lower TWC_{bulk} tests, again perhaps due to the lower nozzle air pressure setting. It can be seen that the melt ratios for the warmer test are higher, which is expected and predicted by the model.

Despite sub-freezing $Twb_{0,i,off}$ and $Twb_{s,e,off}$ values for both data sets, the cloud did not glaciate completely, experimentally or in simulation. The 40-µm MVD_i clouds contained some large particles that did not fully freeze before reaching the tunnel exit. Also, there again exists a positive correlation between the increase in $\Delta Twb_{0,e,exp}$ and increasing TWC_{bulk}, which is captured in simulation. As mentioned before, this trend exists because of the additional energy the gas receives from water temperatures in excess of the wet-bulb temperature.

B. Relative Humidity Sweeps and Comparisons

Three tests were run that varied $RH_{0,i}$ and are listed in the *RH Sweep 1* data set in Table 3. The tests were run simulating a low altitude with TWC_{bulk} = 1.0 g/m^3. As $RH_{0,i}$ increased, the magnitude of $\Delta\omega_{e,exp}$ decreased as did the magnitude of the gas temperature drop. This trend is expected as higher $RH_{0,i}$ values reduce the potential for evaporation, and these trends were captured in the simulation to within 30% of the measured value changes.

Table 3: Relative Humidity Data Set Sweeps

Test Series →	***RH Sweep 1***			***RH Sweep 2***			***RH Sweep 2 Saturated***		
Facility Target Conditions									
$P_{0,i}$ (kPa)	87.2			44.6			44.6		
$P_{s,e,off}$ (kPa)	83.7			42.8			42.8		
v_e (m/s)	85			85			85		
Altitude (km)	1.6			6.8			6.8		
$T_{0,i}$ (°C)	6.6			6.1			6.1		
$T_{s,e,off}$ (°C)	3.0			2.5			2.5		
$RH_{0,i}$ (%)	10	35	50	10	25	50	10	25	50
ω_i (g/kg)	0.70	2.4	3.5	1.3	3.3	6.6	1.3	3.3	6.6
$Twb_{0,i,off}$ (°C)	-2.2	0.6	1.7	-5.6	-3.3	0.0	-5.6	-3.3	0.0
$Twb_{s,e,off}$ (°C)	-4.4	-1.7	-0.6	-7.2	-5.0	-1.7	-7.2	-5.0	-1.7
TWC_{bulk} (g/m^3)	1.0			4.9			4.9		
MVD_i (µm)	15			19			19		
$T_{water,i}$ (°C)	7			7			7		
Simulation vs Experimental Measurement Comparison									
TP#	667	668	669	681	682	683	100681	100682	100683
$RH_{s,e,on,sim}$ (%)	33	68	87	122	121	116	99	99	99
$\Delta\omega_{e,exp}$ (g/kg)	1.3	0.99	0.83	3.6	3.1	1.9	3.6	3.1	1.9
$\Delta\omega_{e,sim}$ (g/kg)	0.92	0.88	0.81	4.6	3.9	2.2	4.1	3.4	1.7
$\Delta\omega_{e,\%diff}$ (%)	-26%	-12%	-3%	27%	28%	17%	14%	11%	-9%
$\Delta T_{0,e,exp}$ (°C)	-3.0	-3.1	-2.4	-7.6	-5.9	-4.2	-7.6	-5.9	-4.2
$\Delta T_{0,e,sim}$ (°C)	-2.3	-2.1	-2.0	-9.7	-7.7	-4.9	-8.3	-6.3	-3.8
$\Delta T_{0,e,\%diff}$ (%)	-24%	-32%	-18%	27%	31%	18%	9%	7%	-9%
$\eta_{e,exp}$ (-)	0.16	0.81	0.82	0.08	0.11	0.74	0.08	0.11	0.74
$\eta_{e,sim}$ (-)	0.00	0.82	1.00	0.00	0.01	0.90	0.00	0.01	0.93
$\Delta Twb_{0,e,exp}$ (°C)	0.3	-0.2	0.0	1.2	1.1	0.5	1.2	1.1	0.5
$\Delta Twb_{0,e,sim}$ (°C)	0.2	0.2	0.2	1.6	1.4	0.5	1.6	1.4	0.5

For TP# 667, where $RH_{0,i}$ = 10%, a value of $\eta_{e,exp}$ = 0.16 was measured, suggesting a mixed phase, but perhaps a nearly glaciated cloud. The simulation predicted a fully glaciated cloud. With below freezing wet-bulb temperatures, $Twb_{0,i,off}$ = -2.2 °C (28 °F) and $Twb_{s,e,off}$ = -4.4 °C (24 °F), a mostly glaciated cloud is expected when the cloud MVD_i is small (15 µm). When $RH_{0,i}$ was increased to 35% for TP# 668, a value of $\eta_{e,exp}$ = 0.81 was measured, suggesting a nearly all liquid cloud. The simulation predicted nearly the same value with $\eta_{e,sim}$ = 0.82. Since the cloud spent most of the time in the slow moving plenum experiencing above freezing conditions with a total wet-bulb temperature of approximately $Twb_{0,i,off}$ = 0.6 °C (33 °F), and then for a brief moment static wet-bulb temperatures as low as $Twb_{s,e,off}$ = -1.7 °C (29 °F) during the acceleration period, it is not expected that much of the cloud would have glaciated. As $RH_{0,i}$ was increased to 50% for TP# 669, $\eta_{e,exp}$ was measured to be 0.82, not very different from the previous test, and again suggesting a mostly liquid or perhaps fully liquid cloud. The simulation predicted a fully liquid cloud. Again, a nearly all liquid cloud is expected since $Twb_{0,i,off}$ = 1.7 °C (35 °F), for which the cloud experiences for much of the duration in the icing tunnel, and for a brief moment experiences a barely freezing static wet-bulb temperature of about $Twb_{s,e,off}$ = -0.6 °C (31 °F) as it exited the tunnel. It is possible that the cloud remained fully liquid as it traveled down the length of the wind tunnel for TP# 669 as wet-bulb temperatures tend to increase slightly when the spray cloud is activated.

A second data set was run where $RH_{0,i}$ was varied, this time at a higher altitude and higher total water content (TWC_{bulk} = 4.9 g/m^3). Simulations of this data set was run in two different ways. The first method allowed the flowing gas to become supersaturated and that data set is labeled *RH Sweep 2* (RH_{sim} > 100%). The second method limits the flowing gas to never exceed saturation (RH_{sim} <= 100%) and is labeled as *RH Sweep 2 Saturated* in Table 3. In the latter simulations, instantaneous condensation is implemented into the algorithm if conditions approach supersaturation so as to not exceed saturation. In the former simulations, supersaturation is considered because it may be possible that as the gas reached near saturation levels in the plenum, and then accelerated in the contraction, the gas static temperature rapidly decreased via isentropic expansion with a mostly unchanged absolute humidity, resulting in possibly supersaturated conditions. The two methods are used to simulate this data set, in an attempt to bound the conditions.

In the *RH Sweep 2* data set, all three simulations exceeded saturation levels at the tunnel exit, with all three values around $RH_{s,e,on,sim}$ = 120%. The simulations in this data set over-predicted the absolute humidity increases and gas temperature decreases by about 30% of the measured values. When simulations were run not allowing supersaturation (*RH Sweep 2 Saturated* data set), the predicted absolute humidity increases and gas temperature decreases were predicted to within 10% of the experimentally measured values. This improvement in prediction suggests that near instantaneous condensation does exist.

The predicted melt ratio matched the measured values quite closely for both data sets. This means that the melt ratio did not change much between the supersaturated and saturated simulations. Again one is able to make general predictions of the melt ratio looking at just the total and static wet-bulb temperatures. For TP# 681 and 682, both wet-bulb temperatures were sub-freezing, so it is expected that a small particle cloud would largely glaciate. For TP# 683, where the cloud experienced near freezing conditions in the plenum at $Twb_{0,i,off}$ = 0 °C (32 °F), and then very briefly experienced at its coldest $Twb_{s,e,off}$ = -1.7 °C (29 °F) during the acceleration portion, it is expected that the particles would be mixed phase. It is also worth pointing out that the cloud went from nearly fully glaciated for TP# 682 where $RH_{0,i}$ = 25%, to nearly fully liquid for TP# 683 where $RH_{0,i}$ = 50%. It is expected that the window to generate a mixed phase cloud using relative humidity as the parameter to control η is smaller for small MVD_i clouds and larger for large MVD_i clouds.

C. Water Temperature Sweeps and Comparisons

Two series of $T_{water,i}$ sweeps are presented in Table 4, where *Twater Sweep 1* tests were conducted with an initial cloud size of MVD_i = 15 µm, and *Twater Sweep 2* was conducted with a cloud of MVD_i = 40 µm. Initial water temperatures were increased to as much as 82 °C (180 °F). The change in humidity was relatively insensitive to the increasing $T_{water,i}$ for both sweeps. The model also predicted this nearly constant absolute humidity increase to within approximately 30% of the measured values. In addition, the drop in gas temperature was also insensitive to the increasing $T_{water,i}$, with the model predicting this insensitivity to within approximately 40% of the measured values. The model actually predicted slightly smaller decreases in gas temperature as nozzle temperature increased, due to the fact that the initially warm cloud transferred its heat to the gas, raising the gas sensible heat. These elevated water temperatures (temperatures greater than *Twb*) also account for the increasing $\Delta Twb_{0,e,sim}$ values as $T_{water,i}$ increased. The small TWC_{bulk} values is the reason for the small $\Delta Twb_{0,e,sim}$ increase and the negligible differences in experimentally measured values of $\Delta Twb_{0,e,exp}$ as $T_{water,i}$ increased.

Table 4: Water Temperature Data Set Sweeps

Test Series →	***Twater Sweep 1***			***Twater Sweep 2***	
Facility Target Conditions					
$P_{0,i}$ (kPa)	87.2			87.2	
$P_{s,e,off}$ (kPa)	83.7			83.7	
v_e (m/s)	85			85	
Altitude (km)	1.6			1.6	
$T_{0,i}$ (°C)	6.6			6.6	
$T_{s,e,off}$ (°C)	3.0			3.0	
$RH_{0,i}$ (%)	10			10	
ω_i (g/kg)	0.70			0.70	
$Twb_{0,i,off}$ (°C)	-2.2			-2.2	
$Twb_{s,e,off}$ (°C)	-4.4			-4.4	
TWC_{bulk} (g/m^3)	1.0			0.78	
MVD_i (µm)	15			40	
$T_{water,i}$ (°C)	7	43	82	43	82
Simulation vs Experimental Measurement Comparison					
TP#	667	690	691	689	692
$\Delta\omega_{e,exp}$ (g/kg)	1.3	1.3	1.4	0.69	0.73
$\Delta\omega_{e,sim}$ (g/kg)	0.92	0.94	0.93	0.47	0.49
$\Delta\omega_{e,\%diff}$ (%)	-26%	-27%	-35%	-32%	-33%
$\Delta T_{0,e,exp}$ (°C)	-3.0	-3.0	-3.3	-1.8	-1.8
$\Delta T_{0,e,sim}$ (°C)	-2.3	-2.1	-2.0	-1.0	-0.9
$\Delta T_{0,e,\%diff}$ (%)	-24%	-29%	-41%	-48%	-50%
$\eta_{e,exp}$ (-)	0.16	0.83	0.83	0.70	0.68
$\eta_{e,sim}$ (-)	0.00	0.00	0.00	0.26	0.34
$\Delta Twb_{0,e,exp}$ (°C)	0.3	0.3	0.4	0.0	0.1
$\Delta Twb_{0,e,sim}$ (°C)	0.3	0.5	0.7	0.4	0.5

The model predicted a fully glaciated cloud for all initial water temperatures in the *Twater Sweep 1* data series, even for the initially high water temperatures for TP# 690 and 691. Rather high melt ratios, however, were experimentally measured for these two tests. The model predicted mixed phase conditions for TP# 689 and 692 in the *Twater Sweep 2* data set, but predicted more glaciated values than what was measured. Further testing and analysis are required to understand this melt ratio discrepancy with respect to warmer $T_{water,i}$ values.

D. Cloud Characterization – Particle Size Comparisons

A total of 11 experiments where particle size data was collected is used to compare with model results. All 11 tests produced clouds with a presumed initial size of MVD_i = 15 µm. Only these smallest particle clouds were capable of being measured by the CDP probe alone as the PSD for these clouds are largely contained within the 2-50 µm range of the probe. The other main experimental conditions varied for these 11 experiments with the minimum and maximum value for each parameter listed in Table 5.

Table 5: Cloud Characterization Test Parameter Ranges

	Min	Max
v_e (m/s)	68	192
$P_{s,e,off}$ (kPa)	32.4	84.1
Altitude (km)	1.6	8.7
$T_{s,e,off}$ (°C)	-29	4
$RH_{0,i}$ (%)	40	50
$T_{water,i}$ (°C)	7	82
TWC_{bulk} (g/m^3)	0.5	1.3

All 11 experiments were run at conditions such that the model predicted potential supersaturation. Therefore, to bound the possible cloud size at the tunnel exit, MVD_e, two simulations were run for each experimental test, one where the tunnel gas was allowed to supersaturate, the second where the gas was limited to never exceed saturation. Figure 5 is a 1:1 comparison graph of the predicted $MVD_{e,sim}$ versus the measured $MVD_{e,exp}$ at the tunnel exit. The red triangles in Figure 5 represent simulations that allowed supersaturation, while the blue circles represent simulations that limited the gas to never exceed saturation. The closer a simulation result matches the experimentally measured $MVD_{e,exp,}$ the closer the marker will be to the 1:1 line.

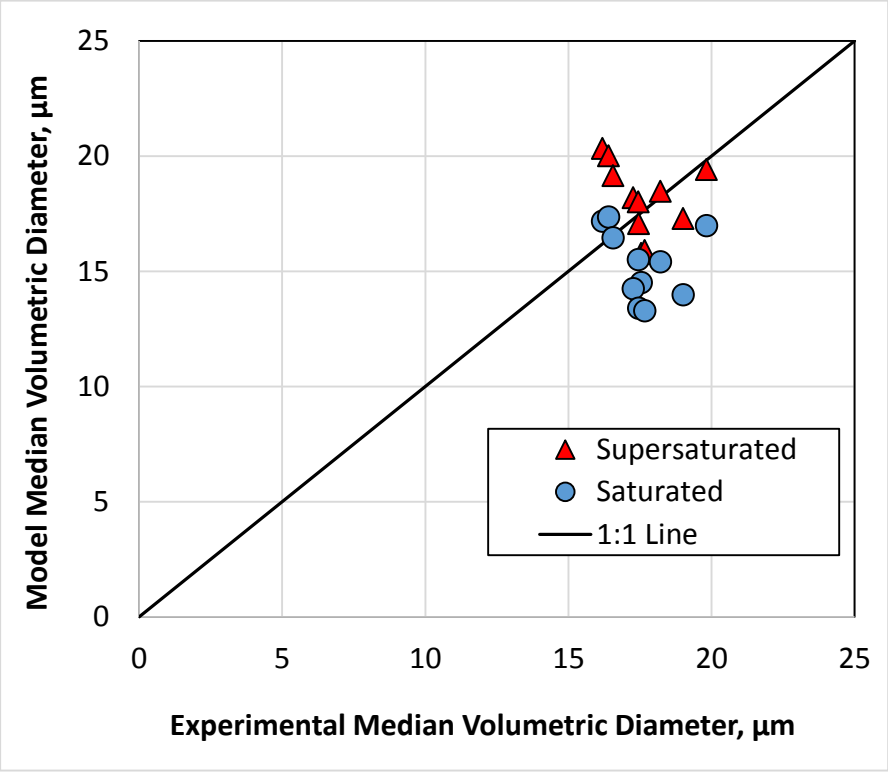

Figure 5: A 1:1 comparison graph of predicted MVD_e values with measured MVD_e values.

In general, the change in particle size was not large, according to experimentally measured values and simulation predictions. With an approximate initial experimental value of MVD_i = 15 µm, the measured final values increased to somewhere between $MVD_{e,exp}$ =16 and 20 µm. The predicted $MVD_{e,sim}$ values for the supersaturated simulations also fall into this 16 to 20 µm range, and generally fall on or above the 1:1 line. The predicted $MVD_{e,sim}$ values for the

saturated simulations range from 13 to 17 μm, and generally fall on or below the 1:1 line. On average, the $MVD_{e,sim}$ values for a supersaturated simulation was about 3 μm larger than saturated simulations.

For the simulations where the gas became supersaturated, the cloud evaporated to the point where the smallest particles completely vaporized, leaving just the largest particles behind. The larger particles also become smaller from evaporative mass losses, but the overall effect mathematically resulted in a larger $MVD_{e,sim}$ values. In addition, particles that glaciated expanded in volume, which also played a role in increasing the cloud $MVD_{e,sim}$ value at the tunnel exit.

The conditions for all 11 experiments, even prior to turning the spray nozzles on, resulted in a potentially supersaturated gas at the tunnel exit due to an isentropic reduction in static temperature. As a result, the cloud would have netted a gain in water mass if the gas was forced to instantaneously condense (IC) so as to never exceed saturation as the cloud moved through the contraction. The IC algorithm distributed the IC mass equally among all of the existing particles. Unlike when evaporation and sublimation increased $MVD_{e,sim}$, condensation and deposition decreased $MVD_{e,sim}$. While all particles increased in volume, the larger share of volume was gained by the smaller particles, mathematically shifting $MVD_{e,sim}$ values below the initial value.

Overall, the model does a fair job in predicting final MVD_e when the initial MVD_i is small. The supersaturated and saturated simulations bound the experimentally measured values to within a few microns. Clouds composed of larger particles were run and measured during the most recent fundamental physics of ice-crystal icing tests at PSL in March 2016. Further simulations are anticipated to be run with these larger MVD_i clouds and compared to the experimental data.

V. Conclusion

The ultimate goal of the model is to better understand the complex interactions between the test parameters and have greater confidence in the conditions at the test section of the PSL tunnel. The model was developed in an attempt to explain the observed changes in test conditions for PSL icing tests by coupling the conservation of mass and energy equations for both the cloud particles and flowing gas mass. When compared to experimental data, the model predicted to within 30% of the measured gas temperature and humidity changes for a variety of parameters. This included variations of total water content, plenum relative humidity, and spray bar water temperatures. A subroutine was implemented that allowed for the option to control humidity so as to not exceed saturation at any point. Model results showed better agreement when supersaturation was not allowed. The model did reasonably well in predicting melt content at the test section, especially for clouds with larger particle sizes. There was some disagreement in melt fraction when initial water temperature was elevated to 43 °C (110 °F) and 82 °C (180 °F). Further testing and analysis is required to determine this discrepancy. In addition, the model predicted particle size at the tunnel exit with good agreement, however, the comparison was limited to clouds of an initial particle size distribution of MVD_i = 15 μm.

One of the key findings from this work is that there was a nearly constant but slight increase in wet-bulb temperature when the spray cloud was activated for every test and simulation. This increase is wet-bulb temperature is attributed to the initial water temperature being warmer than than the wet-bulb temperature. Another finding from this work was that the total wet-bulb temperature in the plenum was a large factor in determining cloud phase. Finally, the model aided the fundamental physics of ice-crystal ice accretion tests in March 2016 in guiding the development of the test matrix and helping to identify the mixed-phase parameter space.

Acknowledgments

The authors wish to acknowledge the financial support for this work by the Advanced Aircraft Icing (AAI) Subproject of the NASA Advance Air Transport Technology Project (AATT) under NASA's, Advanced Air Vehicle's program.

References

[1]Mason, J.G., Strapp, J.W., and Chow, P., "The Ice Particle Threat to Engines in Flight," *44th AIAA Aerospace Sciences Meeting and Exhibit*, AIAA 2006-206, Reno, 2006.

[2]Struk, P.M., Bencic, T., Tsao, J., Fuleki, D. and Knezevici, D.C., "Preparation for Scaling Studies of Ice-Crystal Icing at the NRC Research Altitude Test Facility," *5th AIAA Atmospheric and Space Environments Conference*, AIAA 2013-2675, San Diego, 2013.

[3]Fuleki, D.M., Mahallati, A., Knezevici, D.C., Currie, T.C., and Macleod, J.D., "Development of a Sensor for Total Temperature and Humidity Measurements under Mixed-Phase and Glaciated Icing Conditions," *6th AIAA Atmospheric and Space Environments Conference*, AIAA 2014-2751, Atlanta, 2014.

[4]Struk, P., Currie, T., Wright, W., Knezevici, D., Fuleki, D., Broeren, A., Vargas, M., and Tsao, J., "Fundamental Ice Crystal Accretion Physics Studies", SAE International Technical Paper 2011-38-0018, 2011.

[5]Currie, T.C., Struk, P.M., Tsao, J., Fuleki, D., and Knezevici, D.C., "Fundamental Study of Mixed-Phase Icing with Application to Ice Crystal Accretion in Aircraft Jet Engines," *4th AIAA Atmospheric and Space Environments Conference*, AIAA 2012-3035, New Orleans, 2012.

[6]Willbanks, C.E., and Schulz, R.J., "Analytical Study of Icing Simulation for Turbine Engines in Altitude Test Cells," Arnold Air Force Station Tenn, AEDC-TR-73-144, 1973.

[7]Hindmarsh, J.P., Russell, A.B., and Chen, X.D., "Experimental and numerical analysis of the temperature transition of a suspended freezing water droplet*," International Journal of Heat and Mass Transfer,* Vol. 46, No. 7, 2003, pp. 1199-1213.

[8]Strub, M., Jabbour, O., Strub, F., and Bédéarrats, J.P., "Experimental study and modelling of the crystallization of a water droplet," *International Journal of Refrigeration* Vol. 26, No. 1, 2003, pp. 59-68.

[9]Wright, W.B., Jorgenson, P.C.E., and Veres, J.P., "Mixed Phase Modeling in GlennICE with Application to Engine Icing," *AIAA Atmospheric and Space Environments Conference*, AIAA 2010-7674, Toronto, 2010.

[10]Hauk, T., Roisman, I., and Tropea, C., "Investigation of the Melting Behavior of Ice Particles in an Acoustic Levitator," *AIAA Aviation,* AIAA 2014-2261, Atlanta, 2014.

[11]Villedieu, P., Trontin, P., and Rémi, C., "Glaciated and mixed-phase ice accretion modeling using ONERA 2D icing suite," *AIAA Aviation*, AIAA 2014-2199, Atlanta, 2014.

[12]Bartkus, T., Struk, P., and Tsao, J., "Development of a Coupled Air and Particle Thermal Model for Engine Icing Test Facilities," *SAE Int. J. Aerosp.*, Vol.8, No. 1, 2015, pp. 15-32.

[13]Oliver, M., "Validation Ice Crystal Icing Engine Test in the Propulsion Systems Laboratory at NASA Glenn Research Center," *AIAA Aviation,* AIAA 2014-2898, Atlanta, 2014.

[14]Van Zante, J.F., and Rosine, B.M., "NASA Glenn Propulsion Systems Lab: 2012 Inaugural Ice Crystal Cloud Calibration," *6th AIAA Atmospheric and Space Environments Conference*, AIAA 2014-2897, Atlanta, 2014.

[15]Struk, P., Tsao, J., and Bartkus, T., "Plans and Preliminary Results of Fundemental Studies of Ice Crystal Icing Physics in NASA Propulsion Systems Laboratory," 8th AIAA Atmospheric and Space Environments Conference, AIAA Aviation and Aeronautics Forum and Exposition 2016, American Institute of Aeronautcs and Astronautics, Washington, D.C. (submitted for publication).

[16]Van Zante, J.F., Bencic, T.J., and Ratvasky, T.P., "Update on the NASA Glenn Propulsion Systems Lab Ice Crystal Cloud Characterization (2015)", 8th AIAA Atmospheric and Space Environments Conference, AIAA Aviation and Aeronautics Forum and Exposition 2016, American Institute of Aeronautcs and Astronautics, Washington, D.C. (submitted for publication).

[17]MATLAB Release 2015b, The MathWorks, Inc., Natick, Massachusetts, United States.

[18]Lilie, L., Emery, E., Strapp, J.W. , and Emery, J., "A Multiwire Hot-Wire Device for Measurment of Icing Severity, Total Water Content, Liquid Water Content, and Droplet Diameter," *43rd AIAA Aerospace Sciences Meeting and Exhibit*, AIAA 2005-859, Reno, 2005.

[19]Struk, P.M., Rigby, D.L., and Venkataraman, K., "A Thermal Analysis of a Hot-Wire Probe for Icing Applications," *6th AIAA Atmospheric and Space Environments Conference*, AIAA 2014-2331, Atlanta, 2014.

[20]Rigby, D.L., Struk, P.M., and Bidwell, C., "Simulation of fluid flow and collection efficiency for an SEA multi-element probe," *6th AIAA Atmospheric and Space Environments Conference*, AIAA 2014-2752, Atlanta, 2014.

[21]Van Zante, J.F., Ide, R.F., Steen, L.E., and Acosta, W.J., "NASA Glenn Icing Research Tunnel: 2014 Cloud Calibration Procedure and Results," NASA/TM-2014-218392, 2014.

[22]Veres, J.P., Jorgenson, P.C.E, Wright, W.B, Struk, P., "A Model to Assess the Risk of Ice Accretion due to Ice Crystal Ingestion in a Turbofan Engine and its Effects on Performance," *4th AIAA Atmospheric and Space Environments Conference*, AIAA 2012-3038, New Orleans, 2012.

[23]John, J.E.A., *Gas Dynamics*, Allyn and Bacon, Inc., Boston, 1969, Chap. 5.